Representation of Intermolecular Potential Functions by Neural Networks

Helmut Gassner,[†] Michael Probst,*[,†] Albert Lauenstein,[‡] and Kersti Hermansson[‡]

Institute of General and Inorganic Chemistry, Innsbruck University, Innrain 52a, A-6020 Innsbruck, Austria, and Inorganic Chemistry, The Ångström Laboratory, Uppsala University, Box 538, S-75121 Uppsala, Sweden

Received: July 8, 1997; In Final Form: March 17, 1998

We have investigated how a neural network representation of intermolecular potential functions can be used to elevate some of the problems commonly encountered during fitting and application of analytical potential functions in computer simulations. For this purpose we applied feed-forward networks of various sizes to reproduce the three-body interaction energies in the system $H_2O-Al^{3+}-H_2O$. In this highly polarizable system the three-body interaction terms are necessary for an accurate description of the system, and it proved difficult to fit an analytical function to them. Subsequently we performed Monte Carlo simulations on an Al^{3+} ion dissolved in water and compared the results obtained using the neural network type potential function with those using a conventional analytical potential. The performance and results of our calculations lead to the conclusion that, for suitable systems, the advantages of a neural network type representation of potential functions as a model-independent and "semiautomatic" potential function outweigh the disadvantages in computing speed and lack of interpretability.

1. Introduction

It is now rather commonly appreciated that so-called "artificial neural networks" (which will further be abbreviated as NNs) can be useful in various contexts. Among the most important are storage and interpolation of data as well as pattern recognition in the sense of extracting important features from sets of data. The interest in NNs has increased much during the past decade, although the concept has been known for 50 years.[1,2]

Examples of applications in the field of chemistry include medical chemistry,[3] electrostatic potential comparison,[4,5] and, generally, structure−activity relationship studies of various kinds.[4] Whereas in most such applications semiquantitative results are sufficient and a very accurate reproduction or prediction of data is not necessary, the simple mathematical structure of feed-forward NNs also makes them a suitable alternative for classical function approximation.

Furthermore, due to their relatively simple structure and their universal applicability, NNs can be implemented in computer hardware, and specialized NN coprocessors are available (this is a situation similar to that in the case of digital signal processing). A second technical aspect is that they are very well suited for parallel processing.

The conceptual and practical importance of the potential energy surface (PES) within the framework of "Born−Oppenheimer chemistry" is well established. In the following, we will use the terms "potential energy surface" and "potential energy function" interchangeably. PESs are needed, for example, as input for molecular mechanics, molecular dynamics, and Monte-Carlo simulations. The feasibility of performing such simulations critically depends on an accurate and fast representation of the system energy as a function of the atomic or molecular coordinates. In the many cases where it is not necessary or feasible to calculate energies (or forces) by quantum chemical means, the potential energy surface is commonly approximated by analytical potential energy formulas. These have usually been obtained by parametrization, either toward quantum chemically calculated energies or toward different experimental data, and should allow fast and accurate retrieval and interpolation of the energies and forces. In this sense, analytical potential functions can be viewed simply as a means of storing and retrieving data and to map discrete data points into continuous functions, as can also be accomplished, for example, via interpolation from look-up tables or via splines or Bezier curves.

It often turns out that the fitting procedure to construct such analytical functions is a labor-intensive and cumbersome task which requires a lot of experience since, in a real chemical system, a multitude of bonding effects interact to form the potential surface. From a more formal point of view, the total energy of a molecular system can be expressed as a many-body expansion:

$$E_{\mathrm{tot}} = \sum_i E_i^{(1)} + \sum_{i<j} E_{i,j}^{(2)} + \sum_{i<j<k} E_{i,j,k}^{(3)} + \ldots + \sum_{i<j<k\ldots<n} E_{i,j,k\ldots,n}^{(m)} \tag{1}$$

where, for example, the pair and three-body interactions are

$$E_{i,j}^{(2)} = E_{i,j} - [E_i^{(1)} + E_j^{(1)}] \tag{2}$$

$$E_{i,j,k}^{(3)} = E_{i,j,k} - [E_i^{(1)} + E_j^{(1)} + E_k^{(1)}] - \sum_{i<j} E_{i,j}^{(2)} \tag{3}$$

The total energy is the sum of one-, two-, three- up to many-body energy terms. $E^{(1)}$ denotes the energy of the monomer, and $E^{(2)}$ and $E^{(3)}$ are the two-body and three-body parts of the potential function. In some cases, the nonadditive parts of the interaction potential are relatively small and the sum may be truncated after the second term. This is often done, for example, in simulation studies of water (e.g. refs 15, 16) and other simple liquids and of biomolecules. For many systems, however, the nonadditive contribution to E_{tot} is more important and should

* Corresponding author.
[†] Innsbruck University.
[‡] Uppsala University.

S1089-5639(97)02209-3 CCC: $15.00
Published on Web 05/23/1998

not be neglected. This would be the case, for example, in systems with charged particles which polarize their neighbors and may even transfer charge to them. The resulting change in the interaction between the neighbors means that the additivity approximation breaks down. An example would be a small, highly charged cation hydrated by water molecules. In such a case, simulations using potential functions with only pair interaction terms may lead to erroneous hydration numbers and other qualitatively wrong properties. These effects were, for example, studied by Probst et al. for the hydration of the Be^{2+} ion.[8,9]

It often turns out to be comparatively easy to set up functions that describe the pairwise interactions between molecules. These functions are frequently written in terms of sums of one-dimensional functions of the interatomic distances. It is generally much more difficult to find an analytical function that fits all occurring types of three-body interactions in the system. We therefore decided to experiment with a neural network approach, in contrast to conventional fitting procedures, for the purpose of reproducing the three-body terms in the water−ion interactions in an aqueous ionic system, namely, Al^{3+}(aq).

The main purpose of this paper is to introduce the methodology and to demonstrate its applicability. Nevertheless, results of MC simulations with the approach described here are also presented and discussed briefly, since, to our knowledge, simulation studies on Al^{3+}(aq) have not yet been published.

2. Method

In this paper we use a neural network to construct three-body interaction energy potential functions for Al^{3+}−water interactions. Compared to the normal fitting approach, the following similarities and differences can be noted.

Instead of "inventing" a potential energy function, one decides on the size of the network. The network, in principle, can fit the data as accurately as desired, but problems regarding spurious minima and other artifacts are still possible. One has to abandon the physical interpretability of the various terms in the potential energy expression (for example those with different powers of the distance) because due to the structure of a neural network, there are no separable terms present.

The representation of the numerical values by a neural network consisting of many (tansigmoidal) transfer functions, as discussed below, normally needs more computational effort than the use of an analytical potential function.

In our case, the output from the network is the interaction energy E of the system or rather its three-body part, and the input consists of the interatomic distances. The functional form is of the shape $f(\sum(a_i + b_i x_i))$, where a and b are network-specific parameters and $\bar{x}$ ($\{x_1, x_2, ..., x_n\}$) the input vector or the output of other so-called transfer functions f, which build up the hidden layers inside the network.

Network Architecture. The network architecture[5,10] defines how the different layers are connected to each other. It is, in our case, "feed-forward"; that is, the whole network can simply be expressed as one nested function $E = f(\sum(a_i + b_i f(...)))$, as is visualized in Figure 1. The functions $f(x)$, where x is $\sum(a_i + b_i x_i)$, are in most cases "S-shaped" functions which map x into the ranges $-1 \le f(x) \le +1$ or $0 \le f(x) \le +1$:

$$f(S) = \frac{e^S - e^{-S}}{e^S + e^{-S}} \quad \text{or} \quad f(S) = \frac{1}{1 + e^{-S}} \tag{4}$$

Alternatively they can also be simple scaling functions:

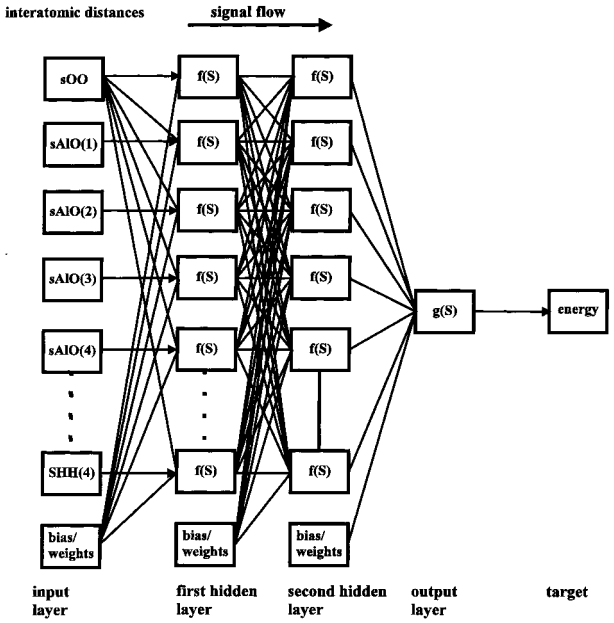

Figure 1. Architecture of the feed-forward network. The input consists of a vector of interatomic distances which are processed to calculate the energy.

$$f(S) = kS \tag{5}$$

For network training we used the back-propagation algorithm. The generalized delta-rule for gradient descent was employed.[11,12] An adaptive learning rate η was used in order to improve the speed of the standard back-propagation algorithm.

For all back-propagation calculations, the network parameters were set as follows. The initial learning rate η was set to 10^{-5}; the momentum constant μ was 0.95. The learning increment and decrement factors were 1.05 and 0.70, respectively. The initial weights and biases were generated using the Nguyen−Widrow initial conditions:[13]

$$W_{ij}^{\text{new}} = W_{ij}^{\text{old}} 0.7^i \sqrt{j} \tag{6}$$

Here j is the index of the current neuron, and i is the index of the current input value (1−15 in our case). W_{ij}^{old} is the combined randomly generated weight and bias matrix, which consists of normalized row vectors.

3. The System

Here we will study the interaction of Al^{3+} with water by means of Monte Carlo simulations, using the neural network for the construction of the $H_2O-Al^{3+}-H_2O$ three-body interactions and a simple analytical potential function for all two-body interactions in the system. Other three-body and higher-order terms were neglected. The $Al^{3+}-H_2O$ interaction is so strong that computer simulations with only pairwise additive forces are inaccurate. In an aqueous Al^{3+} solution, the interaction of Al^{3+} with two water molecules mainly occurs for two different types of geometrical conformations. The first conformation type corresponds to one water molecule residing in the first hydration shell (according to the $Al^{3+}-H_2O$ distance) of the cation with the other water molecule in either the first or the second shell and the O−Al−O angle being larger than 50°. The three-body interaction is here repulsive for nearly all chemically feasible orientations of the water molecules. The value of this interaction depends then mainly on the O−Al−O angle and on both ion−oxygen distances. We will call these conformations *type 1*.[14]

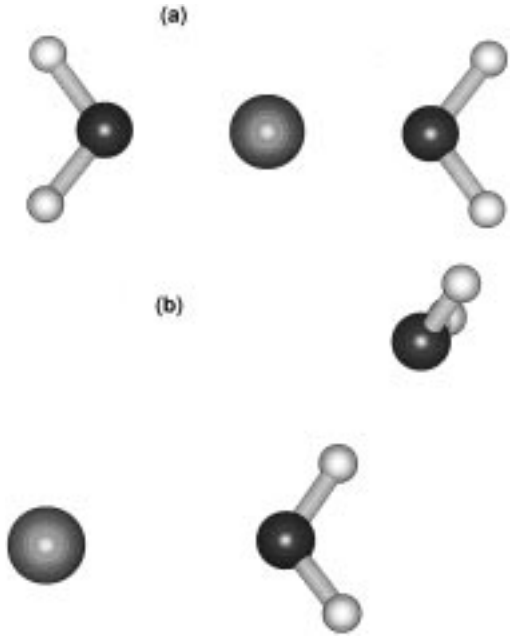

Figure 2. *Type 1* (a) and *type 2* (b) conformations.

If, in contrast, the O−Al−O angle is less than about 50° and one water is located in the first and one in the second hydration shell, we call these conformations *type 2*.[14] Both types of conformations are shown in Figure 2. For *type 2* conformations, the three-body (as well as, of course, the two-body) interaction depends strongly on the relative orientation of the water molecules. The three-body interaction becomes attractive for some orientations, due to the cooperative hydrogen bonding between the water molecules. It is thus necessary to include hydrogen−hydrogen and hydrogen−oxygen interaction terms in the potential energy calculation. For *type 1* conformations, inclusion of the relative orientation of the water molecules in the three-body potential is less important.

Recently Bakker et al.[14] developed a function to reproduce the repulsive O−Al−O three-body energies of the *type 1* conformations by fitting the parameters to about 4500 *type 1* conformations:

$$E^{(3)} = \frac{74.85}{4.187}(0.06413 + (\pi - \alpha)^2)^2 \exp(-0.2465(r_{\mathrm{AlO1}}^2 + r_{\mathrm{AlO1}}^2)) \quad (7)$$

The exponential part takes into account the decrease of the interaction if the Al−O distances increase and the polynomial factor describes the dependence on the O−Al−O angle α. The factors are such that $E^{(3)}$ is in kcal/mol if r is given in Å and α is given in radians. $E^{(3)}$ is always positive. Below we will compare the energies obtained by this function with those from our NN approach. Bakker et al. also generated a large data set of about 8500 *type 2* configurations and corresponding energies. It was found difficult to produce a formula corresponding to eq 7 for fitting these or the combined *type 1* and *type 2* data.

Type 1 and *type 2* conformations were used for the network training. First we trained the network only with the energies of *type 1*, in order to create a potential that could be compared to the analytical function eq 7 mentioned above. Then a combined set of *type 1* and *type 2* was employed as input for the network training.

We thus calculated energies of a data set of about 4500 conformations of *type 1* and about 8500 conformations of *type 2* of the $H_2O-Al^{3+}-H_2O$ system (an exact description of the conformations can be found in ref 14). However, we needed to calculate about 400 new, strongly repulsive, conformations (e.g., with water hydrogens close to Al^{3+} or with hydrogens of different water molecules near to each other). These conformations are essential because the NN is just a powerful interpolating system but was found to fail badly in reproducing energies of conformations that have no similarity to any trained one (extrapolation to "unknown" conformations). Excluding these conformations may lead to artificial minima in the energy calculation. The *type 2* data set was thus augmented with these conformations. All energies were obtained by Hartree−Fock calculations using the same valence double-zeta basis sets with polarization functions as in ref 14, i.e., a modified Huzinaga[25] basis set for Al ([3s2p1d] contraction of a [7s4p1d] primitive set) and the Dunning double-zeta valence bases[26] for O and H. The counterpoise method[17] was used to correct the basis set superposition error.

4. Data Preparation

In the case of energy calculation via a neural network it would be possible to use any internal coordinates that describe the orientation of the molecules in order to implement the orientational dependence of molecule−molecule interactions. For example, quaternions, spherical harmonics, or Euler angles could be used, since it is of minor importance if the energy as a function of these coordinates has a simple shape. For the sake of simplicity, we took interatomic distances as input parameters (Figure 1). They are easy to calculate, and the 15 intermolecular site−site distances in the $Al^{3+}(H_2O)_2$ configurations give a complete—although overdetermined—description of the geometry of the investigated system. The geometry of H_2O was kept rigid during energy calculation and simulation.

Three interatomic distances—for example $Al-O^{(1)}$, $Al-O^{(2)}$, and $O^{(1)}-O^{(2)}$—are required to give a description of the three-body conformation if no information about the mutual orientation is desired. Each additional distance then gives further information about the mutual orientation. In the case of *type 1* conformations, it would thus be sufficient to use the two Al−O distances and the O−O distance to train a neural network to the same or better quality as the analytical potential 7, which just uses these distances. However, it turned out that the network in this first test case—just like potential (eq 7)—could not accurately reproduce all Hartree−Fock energies. Therefore 11 interatomic distances that fully define the spatial conformations were used as input. This set consisted of all Al−O, O−O, O−H, and H−H distances. The comparison between such a neural network trained with data set *type 1* and the analytical three-body eq 7 was our second test case.

The flexibility and applicability of neural networks as an alternative to analytical functions was investigated by augmenting our training set with data of the (mainly) attractive three-body interactions of *type 2*, which describe the interaction between water molecules in different hydration spheres.

In contrast to the situation when conventionally fitted potential functions are used, here the interatomic distances themselves cannot be used as input data. The first reason is simply that, based on the use of tanh(x) as transfer function and Nguyen−Widrow conditioned initial values, the hyperbolic tangent has its inflection point at the origin and remains nearly constant for $x < -1$ and $x > +1$. Hence, both large or small input values lead to very similar output values of nearly −1 or +1, respectively. Therefore, all input values were scaled separately using formula 8:

$$\vec{x}_i^t = \frac{2(x_i^t - x_{\min}^t)}{(x_{\max}^t - x_{\min}^t)} - 1 \quad (8)$$

The calculated scaling parameters were saved and used during the energy calculation to scale the input for unknown conformations. Hence the values of $x_{\min}$ and $x_{\max}$ are part of the network. There are overall 22 values (in the case of 11 input values); t in formula 8 describes the type of interaction, e.g. the first hydrogen−hydrogen interaction. All $x_{\min}$ and $x_{\max}$ values are determined after the symmetrizing operation described in the section below. The prescaling of the input data to values close to or inside the interval $-1 \le \vec{x}_i^t \le +1$ may lead to a problem, since a trained network is normally not capable of reproducing the interaction energy for conformations with distances outside the maximum or minimum distances used in the prescaling factors. If the input distances are outside this predefined range, the scaling does not lead to network inputs within the range between -1 and $+1$. Consequently, all neurons of the first hidden layer will produce values of nearly $+1$ or -1, respectively, and are unable to distinguish between intermediate values. The subsequent layers show the same behavior and produce a meaningless result. Therefore $x_{\min}$ and $x_{\max}$ must be chosen so that not only the distances in the training set but also the distances actually occurring during the simulation are between $x_{\min}$ and $x_{\max}$. For example, if the cutoff distance for three-body interactions is set to 5 Å, the training set should include data for conformations with Al−O distances of at least 5 Å and for O−H distances of at least 10 Å.

The second reason that the interatomic distances themselves cannot be used is the requirement to ensure the correct symmetry of the interactions. As mentioned above, an analytical potential function is normally composed of several terms that describe the interactions between different interaction centers, e.g., the $Al^{3+}\cdots H_{11}$ interaction (H_{11} is H no. 1 on water no. 1). The same terms with the same values of the fitted parameters are used for all interactions between the same type of centers, e.g., for $Al^{3+}\cdots H_{11}$ as well as for $Al^{3+}\cdots H_{12}$, since there is only one class of Al and one class of H atoms. If different fitting parameters would be allowed for the interactions between the same kind of centers, these parameters would not necessarily become equal except in the limit of a complete and infinite data set. In the case of the neural network approach, this simple way to preserve the correct symmetry is no longer possible, since no separate parameters are responsible for each site−site interaction, and one must find a way to ensure that any interchange (Table 1) of two distances between the same class of pair of sites does not change the resulting energy. This can be achieved by applying symmetrization functions to "destroy" the individuality of each distance in the set of distances belonging to the same class of pair of sites. All these functions belong to the same symmetry group D. In our case they can be classified by

$$D = \{(12), (14)(23)(56), (34),(13)(24)(56), (1324)(56), (12)(43), (1423)(56)\} \quad (9)$$

D specifies all allowed cyclic exchanges of atoms where the indices are defined as follows: Al 7, O_1 5, H_{11} 1, H_{12} 2, O_2 6, H_{21} 3, and H_{22} 4. For example, (14)(23)(56) means that two triplets, ($H_{11}/H_{12}/O_1$), ($H_{22}/H_{21}/O_2$), belong to the same class of interactions (Table 1).

The five types of intermolecular distances (a) O−O, (b) Al−O, (c) Al−H, (d) O−H, and (e) H−H must be taken into account (Table 1). A simple way to symmetrize them is to take the absolute value of their sums and differences:

TABLE 1: Symmetry of the System: For Given Cartesian Coordinates These Eight Sets of Atoms Must Lead to the Same Energy. See Text for Further Explanation

Al	Al	Al	Al
$O_1H_{11}H_{12}$ $O_2H_{21}H_{22}$	$O_1H_{12}H_{11}$ $O_2H_{21}H_{22}$	$O_1H_{11}H_{12}$ $O_2H_{22}H_{21}$	$O_1H_{12}H_{11}$ $O_2H_{22}H_{21}$
Al	Al	Al	Al
$O_2H_{21}H_{22}$ $O_1H_{11}H_{12}$	$O_2H_{22}H_{21}$ $O_1H_{11}H_{12}$	$O_2H_{21}H_{22}$ $O_1H_{12}H_{11}$	$O_2H_{22}H_{21}$ $O_1H_{12}H_{11}$

(a) Since there exists only one O−O distance, it can directly be used for the energy calculation.

(b) There are two Al−O distances. In order to assure that an exchange of the O coordinates cannot change the result of the neural network, these distances need to be symmetrized:

$$r_{Al-O}^{(1)} = |r_{Al-O_1} + r_{Al-O_2}| \quad \text{and} \quad r_{Al-O}^{(2)} = |r_{Al-O_1} - r_{Al-O_2}|$$

(c) There are four Al−H distances. The inputs for the allowed interchanges are calculated as the absolute value of two distances of atoms which are allowed to change place combined by plus or minus, respectively. An empirical rule is as follows: combine the distances between the atoms as the sum and the difference of those and take the absolute value of the result. For the more complicated combinations it is necessary to repeat the procedure.

$$r_{Al-H}^{(1)} = |r_{Al-H_{11}} + r_{Al-H_{12}}| + |r_{Al-H_{21}} + r_{Al-H_{22}}|$$

$$r_{Al-H}^{(2)} = |(|r_{Al-H_{11}} - r_{Al-H_{12}}| + |r_{Al-H_{21}} + r_{Al-H_{22}}|) - (|r_{Al-H_{11}} - r_{Al-H_{12}}| + |r_{Al-H_{21}} - r_{Al-H_{22}}|)|$$

$$r_{Al-H}^{(3)} = |(|r_{Al-H_{11}} - r_{Al-H_{12}}| + |r_{Al-H_{21}} + r_{Al-H_{22}}|) + (|r_{Al-H_{11}} - r_{Al-H_{12}}| + |r_{Al-H_{21}} - r_{Al-H_{22}}|)|$$

$$r_{Al-H}^{(41)} = |r_{Al-H_{11}} - r_{Al-H_{12}}| + |r_{Al-H_{21}} - r_{Al-H_{22}}|$$

(d) The situation for the O−H distances is the same:

$$r_{O-H}^{(1)} = |r_{O_1-H_{21}} + r_{O_1-H_{22}}| + |r_{O_2-H_{11}} + r_{O_{21}-H_{12}}|$$

$$r_{O-H}^{(2)} = |(|r_{O_1-H_{21}} + r_{O_1-H_{22}}| + |r_{O_2-H_{11}} - r_{O_{21}-H_{12}}|) - (|r_{O_1-H_{21}} - r_{O_1-H_{22}}| + |r_{O_2-H_{11}} + r_{O_{21}-H_{12}}|)|$$

$$r_{O-H}^{(3)} = |(|r_{O_1-H_{21}} + r_{O_1-H_{22}}| + |r_{O_2-H_{11}} - r_{O_{21}-H_{12}}|) + (|r_{O_1-H_{21}} - r_{O_1-H_{22}}| + |r_{O_2-H_{11}} + r_{O_{21}-H_{12}}|)|$$

$$r_{O-H}^{(4)} = |r_{O_1-H_{21}} + r_{O_1-H_{22}}| + |r_{O_2-H_{11}} - r_{O_2-H_{12}}|$$

(e) The number of intermolecular H−H distances equals those of the O−H distances:

$$r_{H-H}^{(1)} = (|r_{H_{22}-H_{21}} + r_{H_{22}-H_{11}}| + |r_{H_{21}-H_{11}} + r_{H_{21}-H_{12}}|) + (|r_{H_{22}-H_{12}} + |r_{H_{21}-H_{12}}| + |r_{H_{21}-H_{11}} + r_{H_{22}-H_{11}}|)$$

$$r_{H-H}^{(4)} = (|r_{H_{22}-H_{21}} + r_{H_{22}-H_{11}}| + |r_{H_{21}-H_{11}} + r_{H_{21}-H_{12}}|) + (|r_{H_{22}-H_{12}} - r_{H_{21}-H_{12}}| + |r_{H_{21}-H_{11}} - r_{H_{22}-H_{11}}|)$$

$$r^{(2)}_{H-H} = |(|r_{H_{22}-H_{21}} + r_{H_{22}-H_{11}}| + |r_{H_{21}-H_{11}} + r_{H_{21}-H_{12}}|) + (|r_{H_{22}-H_{12}} + r_{H_{21}-H_{12}}| + |r_{H_{21}-H_{11}} + r_{H_{22}-H_{11}}|) + (|r_{H_{22}-H_{21}} + r_{H_{22}-H_{11}}| + |r_{H_{21}-H_{11}} - r_{H_{21}-H_{12}}|) + (|r_{H_{22}-H_{12}} - r_{H_{21}-H_{12}}| + |r_{H_{21}-H_{11}} + r_{H_{22}-H_{11}}|)|$$

$$r^{(3)}_{H-H} = |(|r_{H_{22}-H_{21}} + r_{H_{22}-H_{11}}| + |r_{H_{21}-H_{11}} - r_{H_{21}-H_{12}}|) + (|r_{H_{22}-H_{12}} - r_{H_{21}-H_{12}}| + |r_{H_{21}-H_{11}} + r_{H_{22}-H_{11}}|) - (|r_{H_{22}-H_{21}} + r_{H_{22}-H_{11}}| + |r_{H_{21}-H_{11}} - r_{H_{21}-H_{12}}|) + (|r_{H_{22}-H_{12}} - r_{H_{21}-H_{12}}| + |r_{H_{21}-H_{11}} + r_{H_{22}-H_{11}}|)|$$

5. Determining the Network Structure

The number of adjustable parameters of the neural network is determined by the number of hidden units and by the size of the input vector:

$$n = i(n_i + 1) + j(i + 1) + (j + 1) \qquad (10)$$

In this equation, n is the number of adjustable parameters, i is the number of neurons in the first hidden layer, n_i is the number of input parameters, and j is the number of neurons in the second hidden layer. For example, a network that processes 11 input parameters with five neurons each in the first and second hidden layer and one output neuron has altogether 96 parameters (also called weights and biases). We refer to the size and structure of the network as "5+5+1", or, in general, "i+j+1".

For optimal results, it is important to choose a reasonable number of neurons and inputs. Too many neurons will cause the data set to be "memorized" (the so-called overtraining effect). On the other hand, a network with too few neurons may be insufficient to extract all information from the data set. In practice one has to try different network sizes and monitor the prediction capability and the recall error before deciding on the optimal number of neurons. Table 2 lists the number of floating-point operations for some different network sizes and different sizes of the input vector, and Table 3 shows the corresponding CPU times.

Each network was trained for 20 000 back-propagation cycles using the method of immediate error correction (that means the error correction for all input data is done at once). For simplicity, all networks had the same number of neurons in the first and second hidden layer. As test cases, we trained networks with the preprocessed *type 1* plus *type 2* conformations. Points with energies higher than +100 kcal/mol were removed since their probability is negligible. Half of the remaining data (about 6600 points) was used for network training. The other half was then used in a jackknife test to calculate the prediction error which was examined after each back-propagation cycle in order to recognize a possible overtraining effect.

Table 3 shows the capacity of recalling and predicting energies, respectively. Since the networks are all relatively small, the error of prediction and the error of recall normally decrease with increasing number of neurons. One can see that too few neurons are not able to extract the hidden information accurately; on the other hand, too little information about the conformation of the examined system disables exact differentiation between similar conformations. It can be seen that a network with four or five neurons in each hidden layer is a good compromise between error and computational effort and that the behavior of the prediction error is nearly similar to that of the recall error. As an exception, a slight tendency to an overtraining effect of networks with only three and seven inputs should be mentioned.

TABLE 2: Number of Floating Point Operations (Flops) Required for Calculating One Energy as a Function of the Size of the Network. The Numbers in Parentheses Include Symmetrizing and Prescaling Operations. For Comparison, the Analytical Potential Function[14] Needs 14 (47) Flops

number of neurons	inputs			
	3	**7**	**11**	**15**
1+1+1	24 (62)	32 (146)	40 (254)	48 (326)
2+2+1	54 (92)	70 (184)	86 (300)	102 (380)
3+3+1	86 (124)	110 (224)	134 (348)	158 (436)
4+4+1	122 (160)	154 (268)	186 (400)	218 (496)
5+5+1	162 (200)	202 (316)	242 (456)	282 (560)
6+6+1	206 (244)	254 (368)	302 (516)	350 (628)
7+7+1	254 (292)	310 (434)	366 (580)	422 (700)
8+8+1	306 (344)	370 (484)	434 (648)	498 (776)
9+9+1	362 (400)	434 (548)	506 (720)	578 (856)
10+10+1	422 (460)	502 (616)	582 (796)	662 (940)

TABLE 3: Standardized Errors (kcal/mol) for Recall and Prediction after Training for 20 000 Cycles As Determined by Training of Networks with Different Numbers of Neurons and Input Data. The CPU Time Refers to the Network Training (Time in Minutes on an SGI Indigo 4000 Workstation)

neurons	weights	CPU time	recall error	prediction
		3 Inputs		
1	8	85	13.38	13.58
3	28	223	5.38	5.78
5	56	346	5.18	5.56
7	92	487	4.93	5.75
9	136	644	4.69	5.11
		7 Inputs		
1	12	95	11.74	11.85
3	40	235	4.58	4.75
5	76	361	3.81	3.96
7	120	516	3.36	3.46
9	172	648	3.53	3.66
		11 Inputs		
1	16	114	11.73	11.85
3	52	251	3.87	4.03
5	96	376	3.21	3.32
7	148	520	3.07	3.22
9	208	667	2.59	2.69
		15 Inputs		
1	20	122	11.08	11.25
3	64	265	3.83	4.00
5	116	392	3.16	3.29
7	176	538	3.00	3.12
9	244	688	2.51	2.66

Missing information about the spatial conformation of the examined system necessarily leads to inaccurate reproduction of the energy, but as can be seen from the figures, this effect is gradual. For example, if only the three distances Al−$O^{(1)}$, Al−$O^{(2)}$, and $O^{(1)}$−$O^{(2)}$ are used, the network has no information about the positions of the hydrogens and subsequently even a large network fails to correctly reproduce and predict conformations that differ only in the hydrogen positions. This might not be a serious problem if one is only interested in the repulsive parts of the three-body problem because, as mentioned before, these conformations do not strongly depend on the hydrogen positions. For the fitting of the attractive parts of the potential (the *type 2* data) the relative orientations are important, however. With 11 interatomic distances the system is fully defined and the network accurately reproduces the energies. The use of all 15 interatomic distances does not improve the results any more,

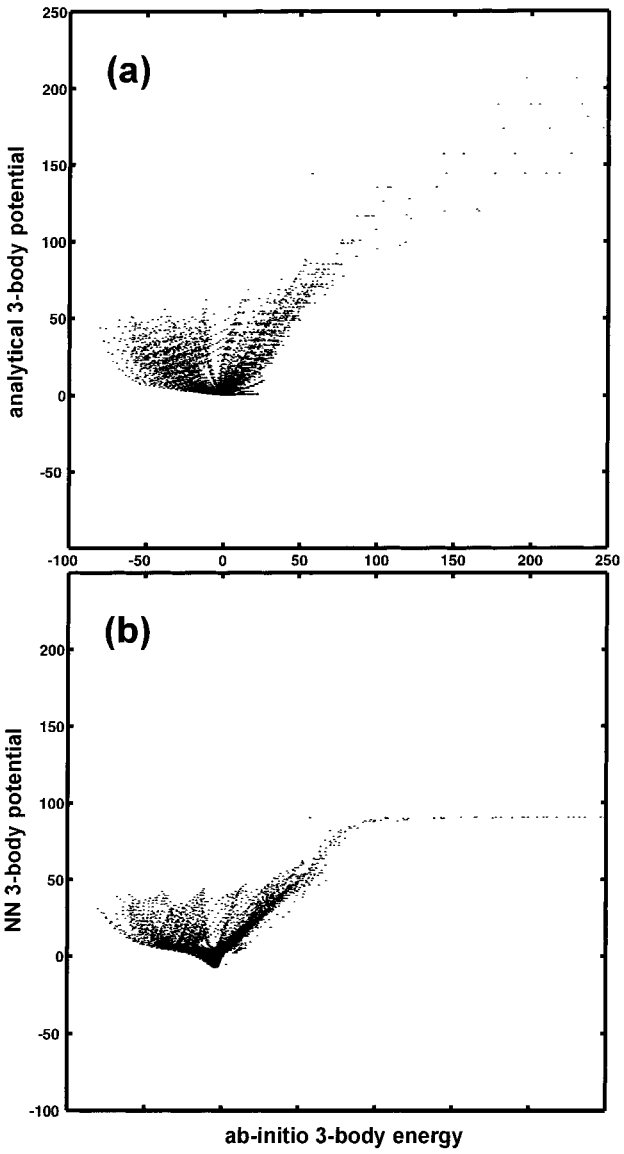

Figure 3. Correlation analysis for the analytical three-body potential (a) and the network potential trained with *type 1* data (b). Because no information about attractive conformations is present, the NN potential fails for *type 2* energies, as does the analytical one.

because it contains redundant information. Hence we decided to use a 5+5+1 network with 11 inputs for the subsequent MC simulations.

6. Results: The Final Potentials

The simulation results presented here are best understood if we first look at the differences of the applied potential functions. Let us briefly reexamine the analytical potential function. Figure 3a shows that the repulsive parts of the three-body interaction (the upper right quadrant) are fairly well reproduced but that the potential function fails for the attractive (*type 2*) interactions, which are caused by the interaction of "hydrogen-bonded" water molecules in different hydration shells with O−Al−O angles less than 50°. Formula 7 has only three arguments—$r(\mathrm{Al-O_1})$, $r(\mathrm{Al-O_2})$, and $\angle(\mathrm{O-Al-O})$—and the resulting energy surface is rather simple. Corresponding to Figures 3a and 3b, in Figure 4a and 4b two-dimensional subsets of the energy surface with one water molecule at a fixed position are shown. The network surface generated using the same (*type 1*) conformations and with $r(\mathrm{Al-O_1})$, $r(\mathrm{Al-O_2})$, and $r(\mathrm{O_1-O_2})$ used as input for the

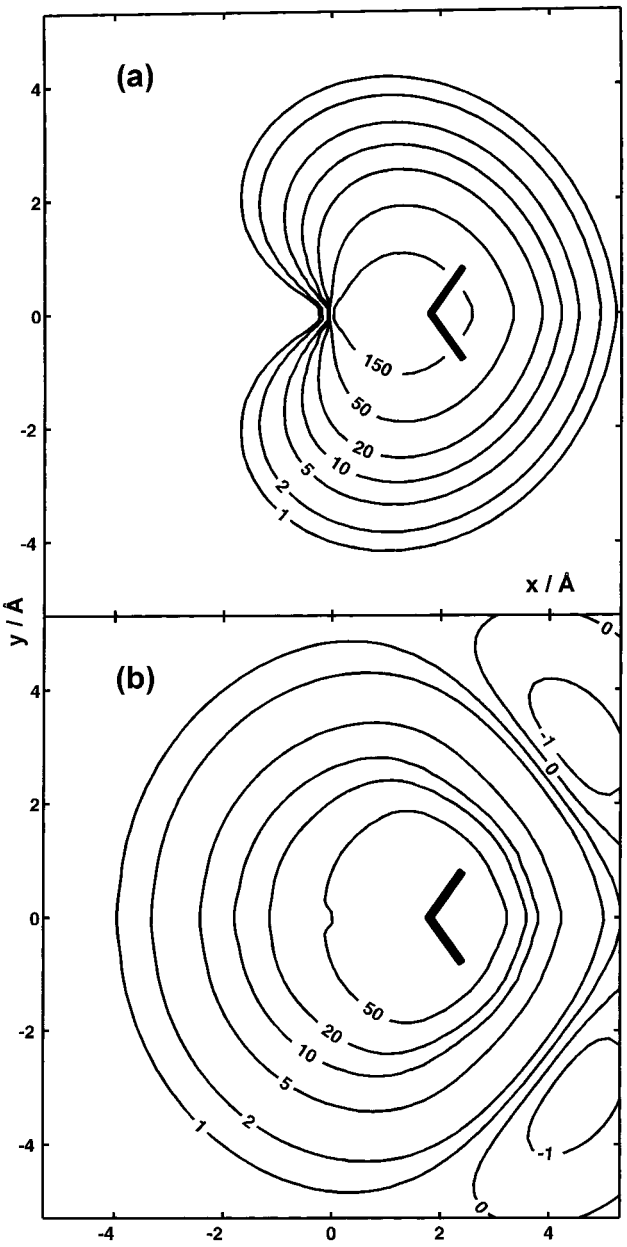

Figure 4. Contour plots of the three-body energy surface of *type 1* conformations (a) calculated using the analytical potential and (b) by a (5+5+1) network trained only with these conformations. In (b) the repulsive parts of *type 1* conformations as well as some slightly attractive conformations of *type 1* are reproduced well. For both (a) and (b) the energy is a function only of the distances of the Al^{3+} ion to the oxygen atoms of the water molecules and the angle formed by these distance vectors.

network trainings is shown in Figure 4b. The main difference between the upper and lower parts of Figure 4 occurs for conformations where both water molecules lie on opposite sides of the Al ion. Here the NN potential is more repulsive than the analytical one (Figure 4a). More contour lines in the low-energy than in the high-energy regions were drawn to show this more clearly in the figures. An examination of the ab initio data points shows that the NN potential reproduces them more faithfully and that the functional form of eq 7 leads to a nearly vanishing three-body potential for $\angle(\mathrm{O-Al-O}) = 180°$, whereas the real one has a minimum but does not vanish.

Figure 3b shows the same correlation for the NN potential as is shown in Figure 3a for the analytical one. The regions with energies in excess of 100 kcal/mol are not reproduced,

since the data threshold was set to this value. Extremely repulsive energies have only little importance during simulations; on the other hand, the reduction of the energy range lowers the amount of neurons needed for accurate energy reproduction. The low overall quality of the fit is again caused by the wrong reproduction of *type 2* energies. There is no difference between the *type 1* and *type 2* energy surfaces of the neural network, a consequence of the number of input parameters. The network has no further information about strongly attractive conformations. Since the input data lack information about O−H and H−H orientations or distances, the network fails to reproduce *type 2* energies and their contour plots would therefore be similar to Figure 4b.

If on the other side both *type 1* and *type 2* conformations with a fully defined data set (11 inputs, including Al−O, O−O, O−H, and H−H distances) are used, the energy surface changes in regions of attractive three-body interactions. *Type 1* and *type 2* energy surfaces calculated using this network are not alike, as shown in Figure 5. *Type 2* conformations have minima in the region of O−H hydrogen bonding. In contrast, *type 1* conformations show a minimum for C_{2v} symmetry with bifurcated hydrogen bonds. The correlation analysis (Figure 6) underlines the accuracy of the fit. It should be mentioned again that it would probably be quite difficult to find an analytical function with the same properties.

7. Monte Carlo Simulations

Details of the Simulations. To demonstrate our approach, Monte Carlo simulations were carried out with a code originating from the program CARLOS[18] adapted and augmented by the neural network and the three-body routines. For the H_2O-H_2O interactions, the MCY potential[19] was used. The $Al-H_2O$ pair interactions were taken from ref 14:

$$V_{Al-O}[\text{kcal/mol}] = \frac{-658.02}{r} - \frac{597.12}{r^2} + 266001\exp(-3.89948r) \quad (11)$$

$$V_{Al-H}[\text{kcal/mol}] = \frac{329.01}{r} + \frac{38.43}{r^2} + 287.458\exp(-0.35461r) \quad (12)$$

For the $H_2O-Al-H_2O$ three-body interactions, either the analytical potential function 7 or one of our neural network potentials was used.

The basic cube contained 200 water molecules and one cation. The examined Al^{3+} ion was fixed in the middle of the cube with a side length of 18.185 Å. Periodic boundary conditions were used. This represents a 0.28 *m* Al(III) salt solution. The simulation temperature was set to 300 K.

Four simulations were carried out: (a) only pair potentials were used for all interactions. These results are provided for comparison; (b) a simulation where the analytical three-body potential 7 was used for $H_2O-Al^{3+}-H_2O$ interactions is included since no simulations with this potential have been published yet; (c) the NN potential trained with only the repulsive (*type 1*) three-body interactions and (d) the NN potential trained with repulsive and attractive interactions (*type 1 + type 2*) were used.

The three-body interactions were smoothly switched off at large distances using a function similar to the one in ref 9.

$$E_{3b} = E_{3b}(1 - \exp(0.5(r_c - r_1)^4))(1 - \exp(0.5(r_c - r_2)^4)) \quad (13)$$

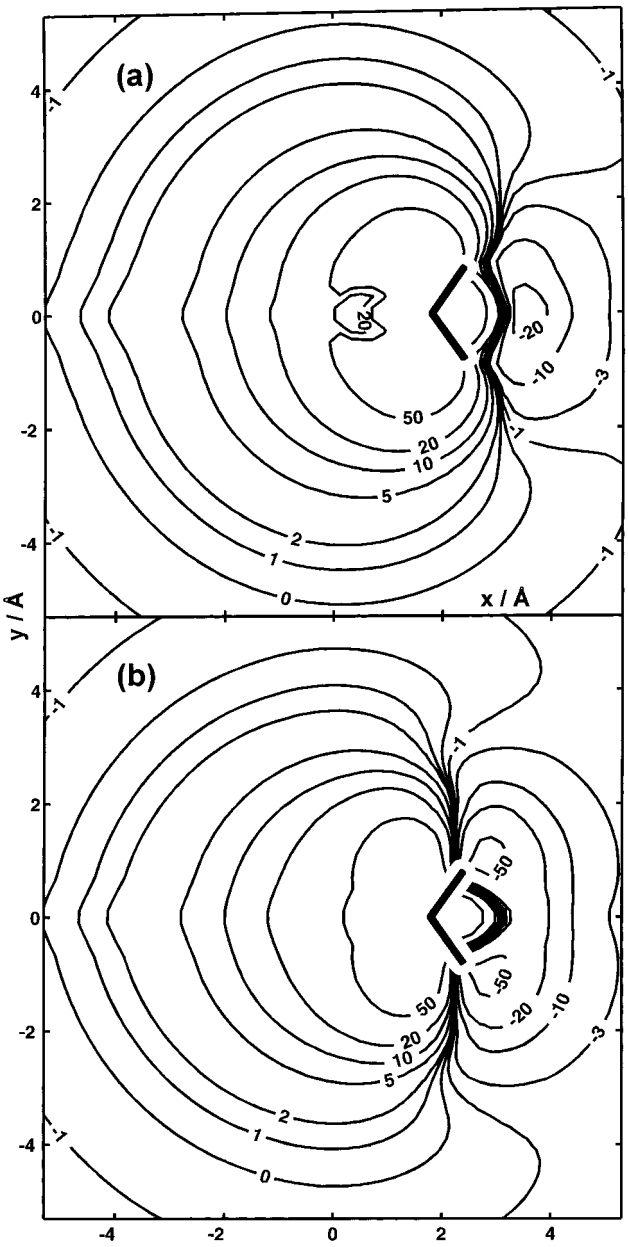

Figure 5. Contour plots of the three-body energy surface of a fully trained (with *types 1 + 2* conformations) network with respect to the reproduction of *type 1* (a) and *type 2* (b) energies. Both the attractive and the repulsive conformations are reproduced accurately.

A cutoff parameter $r_c = 5$ Å was used. After 2×10^6 equilibration cycles 1×10^6 conformations were sampled. The results were collected every 600 moves.

Results of the Simulations. We now compare some representative data extracted from the statistics of the Monte Carlo runs. The hydration shell structure of the cation was calculated in terms of radial distribution functions, $g_{\alpha\beta}(r)$, for the ion−oxygen and ion−hydrogen distances and the corresponding running integration numbers, $n_{\alpha\beta}(r)$:

$$n_{\alpha\beta}(r) = 4\pi\rho_0\int_0^r g_{\alpha\beta}(r)r^2\,dr \quad (14)$$

where ρ_0 is the number density of the atoms of type β. $n_{\alpha\beta}(r)$ up to the first minimum R_{mi} in $g(r)$ gives then the number of coordinating atoms β around atom α. The results are collected in Table 4 in the following order: the results of simulation (b) using pair potentials and the analytical three-body function, the

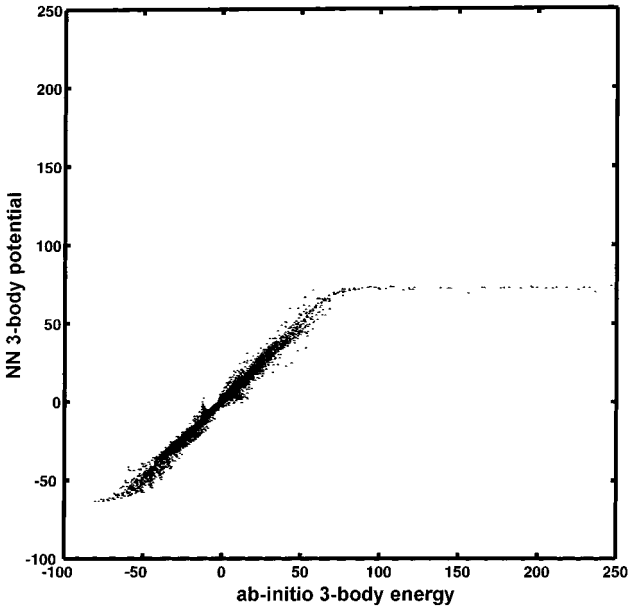

Figure 6. Correlation plot for the fully trained network. A good correlation for repulsive as well as for attractive parts of the interaction is now obtained.

TABLE 4: Values of the Radial Distribution Functions $g_{\alpha\beta}(r)$ for the First Two Hydration Shells of Al^{3+}; r_{m1} and r_{m2} are the Distances (in Å) Where $g_{\alpha\beta}$ Has Its Maximum. R_{mi} Is the Distance of the First Minimum, $g_{\alpha\beta}(R_{mi})$ Is the Value of the Corresponding Radial Distribution Function, and $n_{\alpha\beta}(R_{mi})$ Is the Average Number of α and β at the Minimum Distance R_{mi}

Analytical Three-Body Potential

α	β	r_{m1}	$g_{\alpha\beta}(r_{m1})$	R_{mi}	$g_{\alpha\beta}(R_{mi})$	$n_{\alpha\beta}(R_{mi})$	r_{m2}	$g_{\alpha\beta}(r_{m2})$
Al	O	1.93	26.31	2.18−3.82	0	6	4.19	5.92
Al	H	2.63	10.11	3.10−3.80	0	12	4.91	2.39
O	O	2.81	2.62	3.47	0.87	4.98	4.06	1.11
O	H	1.91	1.15	2.56	0.24	1.90	3.34	1.66
H	H	2.47	1.32	3.12	0.84	5.91	3.86	1.14

NN Potential *Type 1*

α	β	r_m	$g_{\alpha\beta}(r_m)$	R_{mi}	$g_{\alpha\beta}(R_{mi})$	$n_{\alpha\beta}(R_{mi})$	r_{m2}	$g_{\alpha\beta}(r_{m2})$
Al	O	1.98	28.93	2.24−3.87	0	6	4.32	5.28
Al	H	2.65	10.53	3.15−3.75	0	12	4.95	2.38
O	O	2.84	2.54	3.56	0.97	5.61	4.33	1.04
O	H	1.92	1.08	2.50	0.27	1.82	3.34	1.62
H	H	2.48	1.37	3.10	0.84	6.93	3.87	1.13

NN Potential *Type 1 + 2*

α	β	r_m	$g_{\alpha\beta}(r_m)$	R_{mi}	$g_{\alpha\beta}(R_{mi})$	$n_{\alpha\beta}(R_{mi})$	r_{m2}	$g_{\alpha\beta}(r_{m2})$
Al	O	1.91	21.74	2.29−3.52	0	6	3.90	5.84
Al	H	2.62	8.32	3.20−3.75	0	12	4.35/4.40	1.95/2.01
O	O	2.85	2.36	3.68	0.98	6.25	4.16	1.06
O	H	1.92	0.99	2.53	0.28	1.83	3.51	1.50
H	H	2.46	1.42	3.07	0.79	6.61	3.81	1.23

Analytical Two-Body Potential Only

α	β	r_m	$g_{\alpha\beta}(r_m)$	R_{mi}	$g_{\alpha\beta}(R_{mi})$	$n_{\alpha\beta}(R_{mi})$	r_{m2}	$g_{\alpha\beta}(r_{m2})$
Al	O[a]	1.88	26.41	2.46	0	8	4.04	2.58
Al	H[a]	2.60	11.69	3.31	0.06	16	4.55	1.75
O	O	2.84	2.48	3.47	0.87	2.49	4.24	1.09
O	H	1.94	1.09	2.55	0.28	1.96	3.33	1.63
H	H	2.48	1.33	3.05	0.84	6.52	3.81	1.14

[a] A small maximum appearing between the listed first and second maximum includes one water molecule. This fact is explained in ref 14.

results of simulations applying neural potentials of *type 1* (c) and *type 1 + type 2* (d), and the results of simulation (a) using only pair potentials.

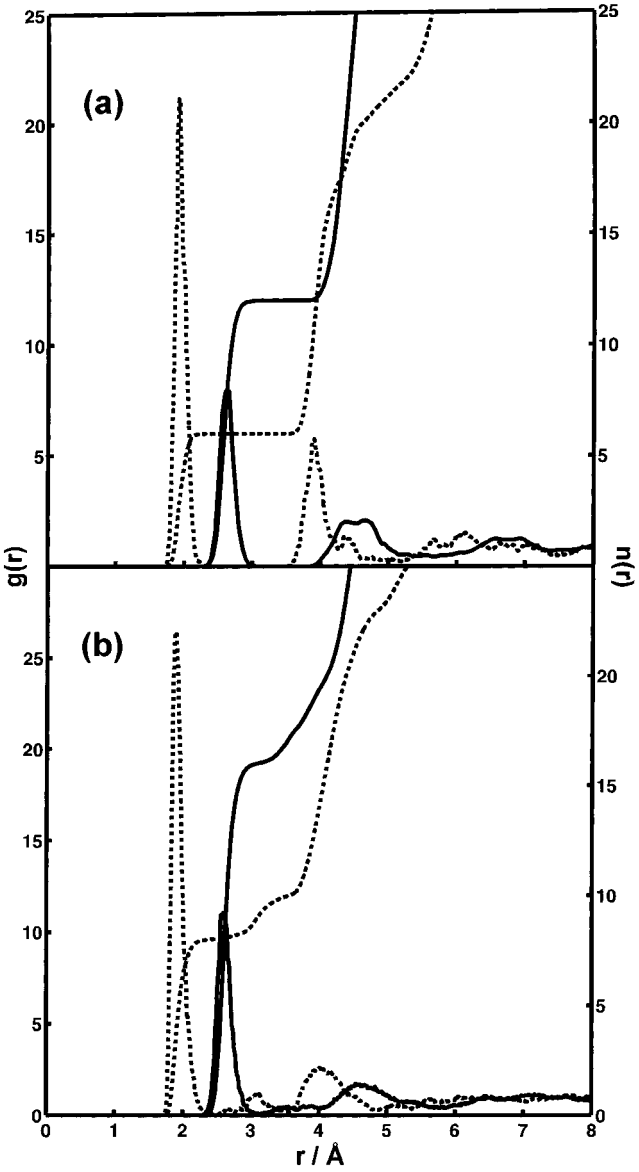

Figure 7. (a) Radial distribution functions of Al−O (dashed line) and Al−H (solid line) from the simulation with a neural network potential (5+5+1) trained with data *types 1 + 2* (MC simulation (d)); (b) using only pair potentials (MC simulation (a)).

Just like with the analytical three-body potential (b), the NN potential functions ensure a coordination number of 6 within the first hydration shell around Al^{3+}; this agrees with the experimentally determined value.[20] The position of the maximum of g_{Al-O} changes from 1.93 (a) to 1.98 Å (c) because of its more repulsive character for the conformations where the O−Al−O angle is nearly linear. Applying the neural network trained with *type 1 + type 2* conformations (d), the Al−O distance decreases to 1.91 Å. This reflects the average influence of the repulsive effects of water molecules within the same hydration shell and the attractive interaction if two water molecules lie within 50° and in different shells. The water molecules of the first and second hydration shell remain well separated during all simulations. Figure 7a shows $g_{Al-O}(r)$ and $g_{Al-H}(r)$ together with their integration numbers for this potential. For comparison, the corresponding curves for the pair potential simulation (a) are included in Figure 7b.

We have analyzed a few other properties that are characteristic of the cationic hydration shell. For comparison, the pair potential data are also given. Figure 8a shows the

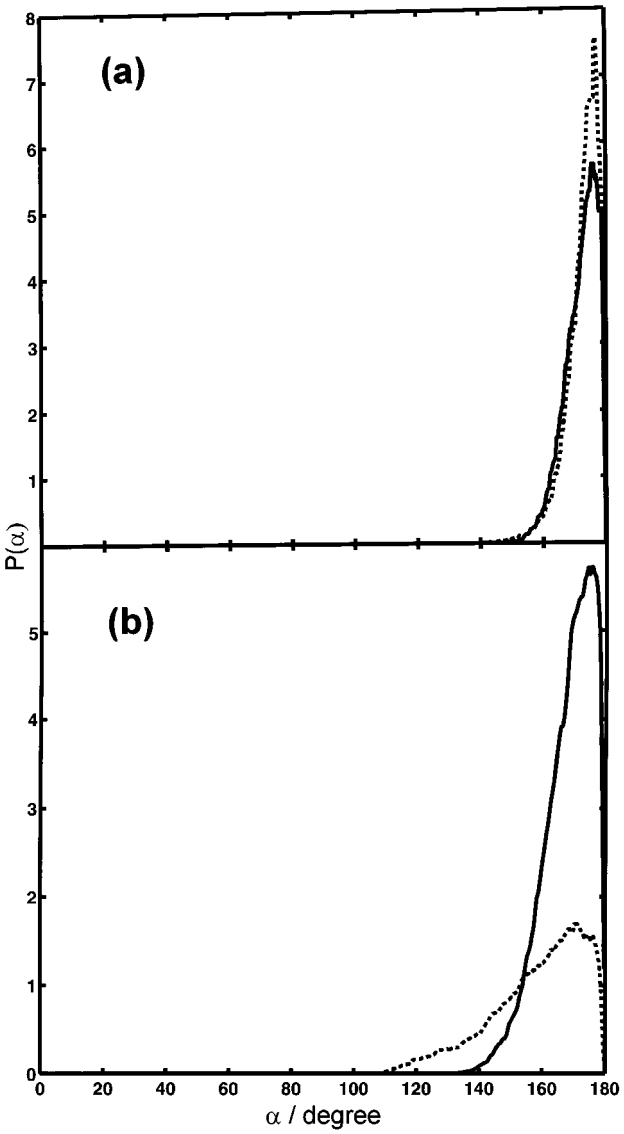

Figure 8. Distribution of the angle between the ion−oxygen distance vector and the dipole vector of water molecules in the first hydration shell for the NN potential simulation c (solid line) and the pair potential simulation a (dashed line) (a) and distribution of the OH···O angle obtained with the neural potential for the same simulations (b).

distribution of the angle between the ion−oxygen vector and the dipole vector of water molecules in the first hydration shell for the pair potential simulation (dashed line) and the neural potential simulation (solid line). Although the water molecules in the latter case are much less tightly bound, the distributions are similar with a maximum close to 180°. This indicates that, due to the decrease in the number of water molecules and the slight increase in Al−O distance, these water molecules have more space and obtain favorable positions. For the same reason, the distribution of the O−H···O hydrogen bond angle (Figure 8b) from the simulation with the neural network potential shows a much sharper maximum around 180° compared with the simple pair potential simulation.

Concerning the second hydration sphere, the position of the second maximum $g(r)$ in simulation (c) changed to 4.32 Å from 4.19 Å determined in the simulation with the analytical potential (b). The NN potential in simulation (d) reduced its value to 3.90 Å as a result of the attractive interactions now included between water molecules of different hydration shells. The g_{OO} radial distribution function (Figure 9) shows a decrease of the average O···O distance from the first to the second hydration

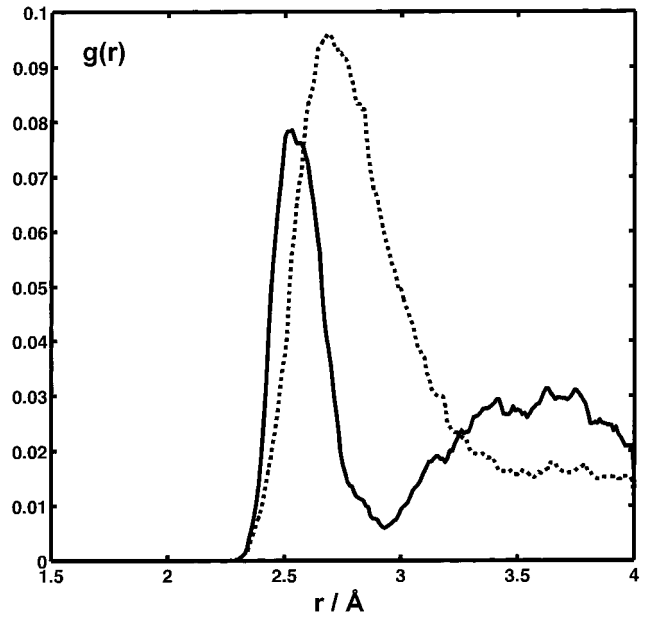

Figure 9. O−O radial distribution function for the subset of water molecules in the first two hydration shells of Al^{3+} for the NN potential simulation c (solid line) and the pair potential simulation a (dashed line).

shell from 2.69 Å (a) to 2.53 Å (d) and a much more structured distribution in the latter case that can be explained by the less crowded hydration shell in the same way as for the angular functions discussed above.

8. Conclusion and Outlook

We have shown that the approach of fitting intermolecular potentials with neural networks is a possible alternative to standard fitting procedures for three-body interaction energies. As a real-world example, the O−Al−O three-body interactions in the Al^{3+}/H_2O system were used. The major advantage and, at the same time, disadvantage is that there are no restrictions imposed by the particular mathematical form of the potential function. A 5+5+1 network should be sufficient for all potential functions between three rigid bodies. The employed back-propagation algorithm with adaptive learning ensures fast and good results with a better ability to interpolate and predict the potential energy of the system than offered by standard analytical potential functions.

It should be kept in mind, however, that neural networks are only one class of functions to model arbitrary hypersurfaces as closely as desired. Other such functions include, for example, certain polynomials, most prominently splines. The relative advantages and disadvantages between these possible candidates are not yet clear, but the current study suggests that feed-forward neural networks have no special "predictive power" for sparsely sampled parts of the energy hypersurface.

The ab initio calculations were carried out using the quantum chemical programs HONDO[21] and Gaussian 90/92.[22] The network training was performed using Matlab 4.2[23] with the neural network toolbox. The simulations were carried out with the Fortran programs mentioned in the text. Coordinates, energies of the data points, and the network parameters are available from the authors upon request as a technical report[24] containing a more detailed description of the neural networks and of the simulations.

Acknowledgment. Support from project 4897 of the Jubiläumsfonds of the Austrian National Bank, the Austrian FWF (project P10106-MOB), and the EEC SCIENCE project SC1

000567 is gratefully acknowledged. We also extend our sincere thanks to Professor Kurt Girstmair from the Institute of Mathematics of Innsbruck University for useful discussions.

References and Notes

(1) McCulloch, W. S.; Pitts, W. *Bull. Math. Biophys.* **1943**, *5*, 115−133.
(2) Pitts, W.; McCulloch, W. S. *Bull. Math. Biophys.* **1947**, *9*, 127−147.
(3) Reibnegger, G.; Weiss, G.; Werner-Felmayer, G.; Judmaier, G. *Proc. Natl. Acad. Sci.* **1991**, *88*, 11426−11430.
(4) Gasteiger, J.; Zupan, J. *Angew. Chem.* **1993**, *105*, 510−536.
(5) Zupan, J.; Gasteiger, J. *Anal. Chim. Acta* **1991**, *248*, 1−30.
(6) Clementi, E.; Kolos, W.; Lie, C. G.; Ranghino, G. *Int. J. Quantum Chem.* **1980**, *17*, 377.
(7) Hermansson, K. *J. Chem. Phys.* **1988**, *89*, 2149−2159.
(8) Probst, M. M.; Spohr, E.; Heinzinger, K. *Chem. Phys. Lett.* **1989**, *161*, 405−408.
(9) Probst, M. M.; Spohr, E.; Heinzinger, K.; Bopp, P. *Mol. Simul.* **1991**, *7*, 43−57.
(10) Kratzer, K. P. *Neuronale Netze Grundlage und Anwendungen*; HANSER-Verlag: München, 1992.
(11) Rumelhard, D. E.; Hinton, G. E.; Williams, R. J. *Nature (London)* **1986**, *323*, 533−536.
(12) Zupan, J.; Gasteiger, J. *Neural Network for Chemists*; VCH Chemie: Weinheim, 1993.
(13) Nguyen, D.; Widrow, B. *Int. Joint Conf. Neural Networks* **1990**, *3*, 21−26.
(14) Bakker, A.; Hermansson, K.; Lindgren, J.; Probst, M. M.; Bopp, P. A. To be published.
(15) Meier, W.; Bopp, Ph.; Probst, M.; Spohr, E.; Lin, J. *J. Phys. Chem.* **1990**, *94*, 4672.
(16) Laurs, N.; Bopp, Ph. *Ber. Bunsen-Ges. Phys. Chem.* **1993**, *68*, 982.
(17) Boys, S. F.; Bernardi, F. *Mol. Phys.* **1970**, *19*, 553.
(18) Collaborative Computational Projects 5, Daresbury Laboratory (http://gserv.dl.ac.uk/CCP/CCP5/librar.html).
(19) Lie, G. C.; Clementi, E.; Yoshimine, M. *J. Chem. Phys.* **1976**, *64*, 2314.
(20) Bergström, P.; Lindgren, J.; Read, M.; Sandström, M. *J. Phys. Chem.* **1991**, *95*, 7650.
(21) Dupuis, M.; King, H. F.; Rys, J. *HONDO 8.0*, IBM Corporation.
(22) Frisch, M. J.; Trucks, G. W.; Head-Gordon, M.; Gill, P. M. W.; Wong, M. W.; Foresman, J. B.; Johnson, B. G.; Schlegel, H. B.; Robb, M. A.; Replogle, E. S.; Gomperts, R.; Andres, J. L.; Raghavachari, K.; Binkley, J. S.; Gonzalez, C.; Martin, R. L.; Fox, D. J.; Defrees, D. J.; Baker, J.; Stewart, J. J. P.; Pople, J. A. Gaussian Inc.: Pittsburgh, PA, 1992.
(23) *Matlab 4.2*; The MathWorks, Inc.: Nantic, MA, 1995.
(24) Gassner, H.; Probst, M.; Lauenstein, A.; Hermansson, K. CCGI Technical Report 2/97.
(25) Huzinaga, S.; Andzelm, J.; Klobukowski, M.; Radzio-Andzelm, E.; Sakai, Y.; Tatewaki, H. In *Gaussian Basis Sets for Molecular Calculations*, Physical Sciences Data 16; Huzinaga, S., Ed.; Elsevier: New York, 1984.
(26) Dunning, T. H. *J. Chem. Phys.* **1970**, *53*, 2823.